2-1-2017

The Effect of Plant Water Storage on Water Fluxes within the Coupled Soil–Plant System

Cheng-Wei Huang
Duke University

Jean-Christopher Domec
Duke University

Eric J. Ward
Oak Ridge National Laboratory

Tomer Duman
Rutgers University - Newark

Gabriele Manolia
Duke University

See next page for additional authors

Accepted version. *New Phytologist*, Vol. 213, No. 3 (February 2017): 1093-1106. DOI.

New Phytologist, Vol. 213, No. 3 (February 2017): 1093-1106. DOI.

The Effect of Plant Water Storage on Water Fluxes within the Coupled Soil–Plant System

Cheng-Wei Huang
Nicholas School of the Environment, Duke University, Durham, NC
Jean-Christophe Domec
Nicholas School of the Environment, Duke University, Durham, NC, USA
Bordeaux Sciences Agro, UMR 1391 INRA-ISPA, Gradignan Cedex, France
Eric J. Ward
Environmental Sciences Division, Oak Ridge National Laboratory, Oak Ridge, TN
Tomer Duman
Department of Biological Sciences, Rutgers University, Newark, NJ
Gabriele Manoli
Nicholas School of the Environment, Duke University, Durham, NC
Anthony J. Parolari
Department of Civil, Construction, and Environmental Engineering, Marquette University, Milwaukee, WI
Gabriel G. Katul
Nicholas School of the Environment, Duke University, Durham, NC, USA
Department of Civil and Environmental Engineering, Duke University, Durham, NC

Summary

- In addition to buffering plants from water stress during severe droughts, plant water storage (PWS) alters many features of the spatio-temporal dynamics of water movement in the soil–plant system. How PWS impacts water dynamics and drought resilience is explored using a multi-layer porous media model.
- The model numerically resolves soil–plant hydrodynamics by coupling them to leaf-level gas exchange and soil–root interfacial layers. Novel features of the model are the considerations of a coordinated relationship between stomatal aperture variation and whole-system hydraulics and of the effects of PWS and nocturnal transpiration ($F_{c,night}$) on hydraulic redistribution (HR) in the soil.
- The model results suggest that daytime PWS usage and $F_{c,night}$ generate a residual water potential gradient ($\Delta\psi_{p,night}$) along the plant vascular system overnight. This $\Delta\psi_{p,night}$ represents a non-negligible competing sink strength that diminishes the significance of HR.
- Considering the co-occurrence of PWS usage and HR during a single extended dry-down, a wide range of plant attributes and environmental/soil conditions selected to enhance or suppress plant drought resilience is discussed. When compared with HR, model calculations suggest that increased root water influx into plant conducting-tissues overnight maintains a more favorable water status at the leaf, thereby delaying the onset of drought stress.

Keywords

drought resilience, hydraulic redistribution, leaf-level gas exchange, nocturnal transpiration, plant water storage, root water uptake

Introduction

The ability of xylem tissues to store water is perceived to be part of an evolutionary process that supports physiological function for the whole plant during severe drought conditions (Tyree & Ewers, 1991; Cruiziat *et al*., 2002; McDowell *et al*., 2008; Manzoni *et al*., 2014; Parolari *et al*., 2014; Sperry & Love, 2015). However, the beneficial effects of plant water storage (PWS) on a wide range of soil–plant hydrodynamic processes have received far less attention. A defining feature of PWS is a time lag between basal sap flux and crown transpiration (Phillips *et al*., 2004; Chuang *et al*., 2006). In large tree species and during severe drought conditions, empirical evidence suggests that a significant amount of whole-plant transpiration originates from PWS (Waring & Running, 1978; Waring *et al*., 1979; Schulze *et al*., 1985; Goldstein *et al*., 1998; Maherali & DeLucia, 2001; Phillips *et al*., 2003). In the presence of PWS, the whole-plant transpiration rate exceeds basal sap flux during the early morning hours, signifying a discharge from PWS. During late afternoon and proceeding into the evening, the basal sap flux can exceed the whole-plant transpiration rate, suggesting partial refilling of PWS and adjustment of xylem pressure to less negative values. These adjustments in xylem pressure may be significant in repairing embolized xylem vessels through bubble dissolution (Waring &

Running, 1978; Tyree & Sperry, 1989; Konrad & Roth-Nebelsick, 2003). Such modifications by PWS beg the question as to how root water uptake (RWU) and hydraulic redistribution (HR) in soils as well as leaf-level transpiration rates are impacted by the presence of PWS. At sites where leaf-level gas exchange occurs, the presence of PWS may allow leaves to maintain a water potential state beneficial to carbon uptake over a longer time period (Goldstein *et al*., 1998; Stratton *et al*., 2000; Maherali & DeLucia, 2001). A daytime dehydration of PWS may also reduce beneficial contributions arising from overnight HR as a result of a competing sink that must be recharged.

One recent review covering the magnitude of HR across a wide range of ecosystems and environmental conditions (Neumann & Cardon, 2012) offers a tantalizing clue that the magnitude of HR predicted by previous models that ignored PWS or nocturnal transpiration ($F_{e,night}$) is consistently higher than those reported by empirical studies. This over prediction of HR occurs despite model differences in the mechanics of incorporating HR (Siqueira *et al*., 2008) or in assumed root density profile properties (Schymanski *et al*., 2008). It was foreshadowed by Neumann & Cardon (2012) that the exclusion of an aboveground competing sink strength (as a consequence of finite PWS or $F_{e,night}$) in such models can be a plausible explanation for the consistent overestimation, which is another motivation for the present work.

The objective of this work was to disentangle the effects of PWS and $F_{e,night}$ on water fluxes from the soil to the leaf from other hydraulic traits on diurnal to daily time-scales. The approach to be used is based on a vertically resolving numerical model for both the soil and plant systems. This model combines soil–plant hydrodynamics with leaf-level physiological and soil–root constraints. Thus, the leaf-level gas exchange can be impacted by soil water availability through the water potential gradient from the leaf to the soil, and vice versa. The focus here is on forested ecosystems where PWS may be significant during an extended dry-down period. The dry-down time-scale is assumed to be sufficiently long to allow PWS to experience multiple discharge–recharge phases under different soil moisture states but sufficiently short so that hydraulic, eco-physiological attributes, leaf area, root distribution, and concomitant allometric properties do not vary appreciably. The model results are then analyzed with particular attention to exogenous environmental factors and endogenous plant attributes promoting the use of PWS vs direct soil water in eight scenarios. While a large number of hydrological and ecological studies have already documented the benefits of HR on carbon–water relations (Domec *et al*., 2010; Prieto *et al*., 2012), conditions where plant hydraulic capacitance or $F_{e,night}$ may compete with HR remain unclear. Hence, the overnight competition for water between above- and belowground reservoirs is discussed through model calculations. The discussion of the model results finally focuses on the responses of leaf-level gas exchange to progressive drought conditions in the context of the functional role of PWS vs HR. For model evaluation, the two-layered sap flux and soil

moisture data collected within a *Pinus taeda* L. stand at the Duke-FACE (free-air CO_2 enrichment) site are also employed.

Description

Modeling framework

There is a plethora of complications when modeling or measuring plant water relations in forested ecosystems, including inhomogeneity in leaf arrangements, the plant and soil hydraulic properties, the rooting system, and the temporal variability in environmental variables. Moreover, plant–plant interactions such as competition for light or water and the dynamic nature of plant hydraulic and physiological properties over long time-scales (e.g. seasonal) necessitate an intermediate level of modeling approaches, as discussed elsewhere (Bohrer *et al*., 2005). In this approach, the bulk water movement along the primary pathways is modeled with much of the finer scale spatial processes (e.g. cavitation and soil–root contact) being surrogated to nonlinearities in hydraulic properties. Hence, within each of the soil–plant compartments, the goal is to retain sufficient representation of key hydrodynamic and physiological processes while allowing for integration to the plant level.

Starting with the aboveground plant compartment, a logical choice is to adopt a 'macroscopic' (i.e. tissue-level) approach in analogy to the soil system. The bulk effect of 'microscopic' processes (i.e. cell or pore level) is embedded in the shape of the vulnerability curve and PWS as they relate to xylem water potential. It is to be noted that xylem conduits are more elongated and their diameters are less variable compared with soil pores. Despite this pore structure difference, the flow and energy losses to friction can still be reasonably approximated by Darcy's law. Hence, a one-dimensional porous medium model is employed to describe the transient water flow from the stem base to the leaf parameterized with literature-reported hydraulic attributes of plant tissues. The soil water supply to the plant is represented using a conventional multi-layered scheme that employs Richard's equation adjusted by soil–root interactions reflecting root water influx or efflux (i.e. possible HR). These interfacial transfer processes depend on soil-to-root conductances along the flow path and the lateral energy gradient between the soil and the neighboring root at a given depth.

The porous-medium analogy representing water flow through each compartment of the soil–plant system and connections between them is capable of capturing the main features of macroscopic water flow pertinent to PWS dynamics. The complex features of plant hydraulic architecture are not explicitly resolved but the effects of tree size, diameter tapping and vertically non-uniform root distribution on plant water relations are captured. The leaf-level water balance employed here provides a representation accounting for the nonlinear relationship between stomatal aperture and the time-history of leaf water potential. The latter is limited by soil water availability and the interplay between

biological controls through stomata and the aerodynamic modifications depending on mean wind speed. This modeling approach is illustrated in Fig. 1and detailed information of the formulations and assumptions is given next. The notation and units used throughout are listed in Table 1.

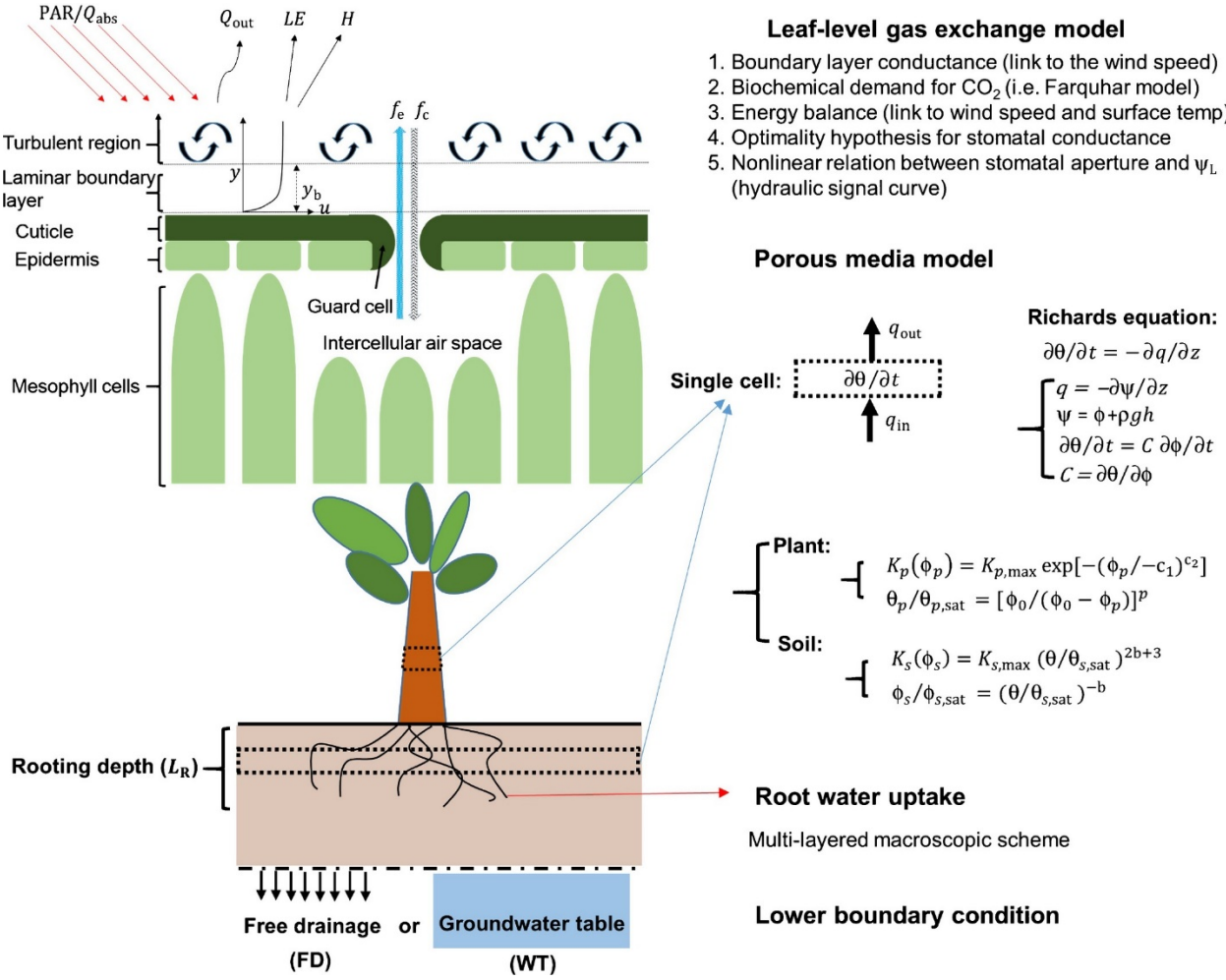

Figure 1. Schematic of the modeling approach describing the water movement through each compartment of the soil–plant system with a summary of the porous medium flow equations used, the lower boundary conditions and the upper boundary conditions forced on the leaf gas exchange equations. For definitions of variables, see Table 2.

Table 1. Nomenclature

Symbol	Description	Unit
A_s	Sapwood area	m^2
$A_{s,base}$	Sapwood area at stem base	m^2
A_{soil}	Soil surface area covering the roots	m^2

Symbol	Description	Unit
A_l	Leaf area	m^2
a_R	Root surface density	$m^2\ m^{-3}$
B	Root length density	$m\ m^{-3}$
b	Empirical constant for soil water retention curve and hydraulic conductivity function	Dimensionless
C_p	Specific hydraulic capacitance	$kg\ m^{-3}\ MPa^{-1}$
$C_{p,total}$	Whole-plant hydraulic capacitance	$kg\ MPa^{-1}$
C_l	Hydraulic capacitance of the leaf	$kg\ m^{-3}\ MPa^{-1}$
C_{uptake}	Total carbon uptake during T_e	$kg\ m^2$
c_a^*	Reference atmospheric CO_2 concentration for λ–$\overline{\Psi}_l$ relation	ppm
c_1	Constant describing the shape of the vulnerability curve	MPa
c_2	Constant describing the shape of the vulnerability curve	Dimensionless
F_e	Total crown transpiration flux	$kg\ s^{-1}$
$F_{e,night}$	Nocturnal transpiration	$kg\ s^{-1}$
f_e	Leaf-level assimilation rate	$\mu mol\ m^{-2}\ s^{-1}$
f_e	Leaf-level transpiration rate	$mol\ m^{-2}\ s^{-1}\ kPa$
g_{res}	Residual conductance accounting for water leakage through guard cells and cuticle overnight	$mol\ m^{-2}\ s^{-1}$
g_{s,CO_2}	Stomatal conductance to CO_2	$mol\ m^{-2}\ s^{-1}$
g	Gravitational acceleration	$m\ s^{-2}$
H	Tree height	m
h_a	Hamiltonian	$\mu mol\ m^{-2}\ s^{-1}$

Symbol	Description	Unit
K_p	Plant hydraulic specific conductivity	kg m^{-1} s^{-1} MPa^{-1}
$K_{p,max}$	Maximum plant hydraulic specific conductivity	kg m^{-1} s^{-1} MPa^{-1}
K_s	Soil hydraulic conductivity	m s^{-1}
$K_{s,max}$	Saturated soil hydraulic conductivity	m s^{-1}
k	Total soil-to-root conductance	s^{-1}
k_r	Root membrane permeability	s^{-1}
k_s	Conductance associated with the radial flow within the soil to the nearest rootlet	s^{-1}
L_R	Rooting depth	m
l	Length scale characterizing the mean radial distance for the movement of water molecules from the bulk soil to the root surface within the rhizosphere	m
m_v	Molecular weight of water (1.8×10^{-2})	kg mol^{-1}
P_{12}	Air- entry point	MPa
P_c	Critical xylem water potential	MPa
p	Constant describing the shape of the plant retention curve	Dimensionless
Q_r	Root water uptake (Q_r^+) or release (Q_r^-) per unit soil volume	s^{-1}
q_p	Sap flow rate	kg s^{-1}
$q_{p,sb}$	Sap flow rate at the stem base	kg s^{-1}
$q_{p,top}$	Sap flux entering the leaf	kg s^{-1}
q_s	Darcian flux	m s^{-1}
RWU_{net}	Net root water uptake	kg s^{-1}
r	Effective root radius	m

Symbol	Description	Unit
r_l	Leaf lamina resistance expressed on a leaf area basis	$kg^{-1}\ m^2\ s\ MPa$
T_c	The duration of a finite $g_{s,CO2}$	d
t	Time	s
V_s	Sapwood volume	m^3
z	Height above ground	m
z_s	Depth below soil surface	m
Δz_l	Effective leaf thickness	m
θ_p	Plant (or xylem) water content on a sapwood volume basis	$kg\ m^{-3}$
$\theta_{p,sat}$	Plant (or xylem) water content at near saturation	$kg\ m^{-3}$
θ_s	Soil water content	$m^3\ m^{-3}$
$\theta_{s,sat}$	Near-saturated soil water content	$m^3\ m^{-3}$
ψ_l	Leaf water potential	MPa
$\overline{\psi_l}$	An averaged ψ_l over the previous 24 h	MPa
$\overline{\psi_{l,c}}$	Critical $\overline{\psi_l}$ leading to a gradual stomatal closure	MPa
ψ_p	Total xylem water potential	MPa
ψ_r	Root water potential	m
ψ_s	Total soil water potential	m
ψ_{sb}	Water potential at the stem base	m
$\Delta\psi_{p,night}$	Residual water potential gradient along the plant vascular system overnight (i.e. above-ground competing sinks)	MPa
ϕ_p	Xylem matric potential	MPa
ϕ_0	Constant describing plant retention curve	MPa
ϕ_s	Soil matric potential	m

Symbol	Description	Unit
$\phi_{s,sat}$	Soil air entry water potential	m
λ	Marginal water-use efficiency	µmol mol^{-1}kPa^{-1}
λ^*	Parameter for λ–$\overline{\psi_l}$ relation	µmol mol^{-1}kPa^{-1}
β	Parameter for λ–$\overline{\psi_l}$ relation	MPa^{-1}
ρ	Water density	kg m^{-3}

Plant conducting tissues

Water transport through tracheid aggregates or vessels inter-connected by end-wall pits in the water-conducting tissues can be treated as analogous to porous medium flow (Edwards *et al*., 1986; Tyree, 1988; Früh & Kurth, 1999; Kumagai, 2001; Aumann & Ford, 2002; Bohrer *et al*., 2005; Chuang *et al*., 2006; Hentschel *et al*., 2013; Manzoni *et al*., 2013a,c, 2014). Thus, a mass conservation equation is combined with Darcy's law to describe the water movement at the tissue-scale and is given as:

$$\frac{\partial V_s(z)\theta_p(z,t)}{\partial t} = -\frac{\partial q_p}{\partial z}dz$$
$$q_p = -A_s(z)K_p(\theta_p)\frac{\partial \psi_p}{\partial z}$$
$$\psi_p = \phi_p + \rho g z, \quad \text{(Eqn 1)}$$

$V_s(z) = \int_z^{z+\Delta z} A_s(z)\mathrm{d}z$ is the sapwood volume between height *z* and *z* + Δ*z* above the soil surface, θ_p is the plant (or xylem) water content, $q_p(z)$ is the sap flow rate driven by gradients in total water potential ψ_p, ρ is the water density, *g* is the gravitational acceleration, K_p is the plant hydraulic specific conductivity, and $A_s(z)$ is the sapwood area profile representing the effective cross-sectional area of conducting tissues. ψ_p includes plant pressure potential (i.e. xylem matric potential) ϕ_p and the gravitational potential ρ*gz* but ignores the kinetic energy head and assumes negligible variations in osmotic potential for long-distance water flow in the xylem (Früh & Kurth, 1999). A cone-shaped tree volume is adopted to represent the effective tree dimensions using only tree height (*H*) and $A_s(z)$ which is linked to *H* by:

$$A_s(z) = A_{s,\mathrm{base}}\left(1 - \frac{1}{2}\frac{z}{H}\right)^2, \quad \text{(Eqn 2)}$$

where $A_{s,\mathrm{base}}$ is the sapwood area at stem base.

In the plant vascular system, the percentage of K_p loss referenced to the maximum specific conductivity $K_{p,\max}$ at near saturation $\theta_{p,\mathrm{sat}}$ as a result of a reduced Φ_p is commonly described by the *vulnerability curve*:

$$K_p(z) = K_{p,\max}\exp\left[-\left(\frac{-\phi_p(z)}{c_1}\right)^{c_2}\right], \quad \text{(Eqn 3)}$$

where c_1 and c_2 are constants describing its shape. The monotonic relationship between θ_p and Φ_p is approximated by a *plant retention curve* and is given by Chuang *et al*. (2006):

$$\frac{\theta_p(z)}{\theta_{p,\mathrm{sat}}} = \left(\frac{\phi_0}{\phi_0 - \phi_p(z)}\right)^p, \quad \text{(Eqn 4)}$$

where p and Φ_0 are constants. This formulation ensures $\Phi_p = 0$ at near saturation and represents the degree of relative change in θ_p with respect to Φ_p through p. The plant 'retention curve' can be further used to infer the specific hydraulic capacitance of a plant tissue $C_p = \partial\theta_p/\partial\phi_p$ by which the whole-plant hydraulic capacitance $C_{p,\mathrm{total}} = \int_0^H A_s C_p dz$ can be defined to describe the ability to store or extract water for a unit change in Φ_p.

Unlike soils, there are a number of potential mechanisms responsible for changes in PWS. These include elasticity, capillarity and cavitation release. They were proposed by Zimmermann (1983) and experimentally shown by Tyree & Yang (1990) to be present in woody cells (i.e. xylem conduits). Unlike living cells (e.g. phloem), woody cells have rigid walls with high elastic modulus so that the elastic storage in xylem conduits resulting from alternating shrinkage and swelling may be minor (Brough *et al*., 1986). Capillary storage, which occurs in cavitated conduits, can release water by bringing the menisci towards the narrow ends of tracheids or vessels when water potential decreases. When the menisci move in the opposite direction with increasing water potential, water refills the capillary storage. This implies that the water continuum can still be maintained in parts of the cavitated conduits (Tyree & Zimmermann, 2002). As capillary storage can rapidly release or store water,

Brough *et al*. (1986) demonstrated that the diurnal pattern of the xylem water content can be attributed mainly to such a capillarity mechanism. Under sufficiently low water potential conditions, water release through cavitation events occurs when the water-filled volume is rapidly replaced by air bubbles (Tyree & Sperry, 1989; Tyree *et al*., 1994). The delay in repair of cavitated conduits can induce hysteresis in both vulnerability and plant retention curves (Sperry & Tyree, 1990; Brodribb & Cochard, 2009), which is not considered here but can be accommodated in the present framework.

Macroscopically, PWS adjusts $\psi_p(z)$ along the plant vascular system and thus impacts stomatal behavior. Stomatal closure occurs before $\psi_p(z)$ is substantially reduced and reaches an apparent threshold that causes 'runaway cavitation' (Bond & Kavanagh, 1999; Sparks & Black, 1999). If this threshold is reached without stomatal closure, the more negative water potential required to maintain transpiration further leads to more dysfunctional xylem conduits as a result of embolism and does so in an irreversible manner. As shown in Fig. 2(a), the incipient runaway cavitation is commonly defined at ϕ_p where 12% of K_p losses occur (i.e. air-entry point; P_{12}). The slope of the vulnerability curve reaches a maximum around this threshold (Domec & Gartner, 2001). However, the onset of water stress sensed by plants (i.e. stomatal closure) is dictated by a critical xylem water potential (i.e. P_c) that may be larger than P_{12}. It is to be noted that P_c and the corresponding loss of K_p are not *a priori* specified here (see section 'Leaf-level water balance').

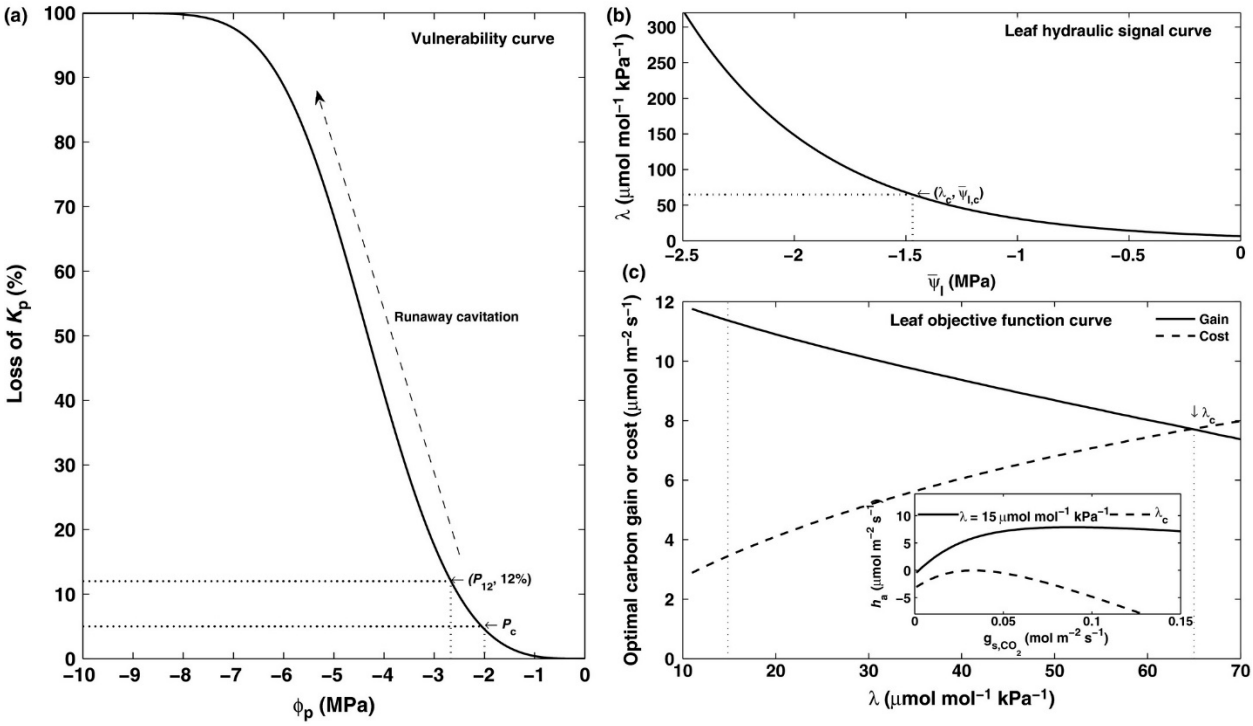

Figure 2. (a) Xylem vulnerability curve with indication of water potentials at 12% loss of plant hydraulic specific conductivity (K_p) (i.e. P_{12}) and at complete stomatal closure (i.e. P_c). (b) The marginal water-use efficiency (λ)

values as a function average leaf water potential over the previous 24 h ($\overline{\Psi}_l$) (Manzoni *et al*., 2011). (c) The two components (i.e. carbon gain and water loss in carbon units) of the optimal 'net' carbon gain (h_a) as a function of λ. Inset: the 'net' carbon gain (h_a) as a function of given stomatal conductance to CO_2 (g_{s,CO_2}) for λ = 15 μmol mol^{-1} kPa^{-1} and λ_c. Note that λ_c, $\overline{\Psi}_{l,c}$ and P_c are determined at the condition where the optimal 'net' carbon gain is identical to zero (i.e. optimal $h_a = 0$). λ = 15 μmol mol^{-1} kPa^{-1} is arbitrarily selected to illustrate that $h_a > 0$ when $\lambda < \lambda_c$.

Soil–root interaction

Water transport in unsaturated soils is described by the one-dimensional Richards' equation modified to include water uptake/release by the rooting system within each soil layer. Hence, at each soil layer, an 'effective' source-sink term Q_r is added (Volpe *et al*., 2013; Manoli *et al*., 2014; Bonetti *et al*., 2015) to yield:

$$\frac{\partial \theta_s(z_s,t)}{\partial t} = -\frac{\partial q_s}{\partial z_s} - Q_r(z_s,t)$$
$$q_s = -K_s(\theta_s)\frac{\partial \psi_s}{\partial z_s}$$
$$\psi_s = \phi_s - z_s, \quad \text{(Eqn 5)}$$

where θ_s is the soil water content at depth z_s below the soil surface, q_s is the Darcian flux driven by the vertical gradient of total soil water potential ψ_s, ϕ_s is the soil matric potential, K_s is the soil hydraulic conductivity, and Q_r is the water uptake (denoted by superscript ' + ') or release (denoted by superscript '–') rate from roots. In Eqn 5, the Clapp and Hornberger formulations (Clapp & Hornberger, 1978) are used to represent the soil water retention curve and soil hydraulic conductivity function, and are given by:

$$\phi_s = \phi_{s,sat}\left(\frac{\theta_s}{\theta_{s,sat}}\right)^{-b}, \quad \text{(Eqn 6)}$$

$$K_s = K_{s,max}\left(\frac{\theta_s}{\theta_{s,sat}}\right)^{2b+3}, \quad \text{(Eqn 7)}$$

where $\theta_{s,sat}$, $\phi_{s,sat}$ and $K_{s,max}$ are the near-saturated water content, air entry water potential and saturated hydraulic conductivity, respectively, and *b* is an empirical constant that varies with soil texture.

The contributions to soil water storage (i.e. $\partial\theta_s/\partial t$) from the gradient of the flux is referred to as the *Darcian redistribution* (i.e. $-\partial q_s/\partial z_s$). The depletion or replenishment rate of soil water storage through Q_r is determined by the water potential gradient across the root membrane and the average path length traveled radially by water molecules from the soil to the soil–root interface in series and is given as:

$$Q_r = -k\left[(\psi_{sb} - z_s) - \psi_s\right] a_R$$
$$k = \frac{k_r k_s}{k_r + k_s}, \quad \text{(Eqn 8)}$$

where k is the total soil-to-root conductance, ψ_{sb} is the water potential at the stem base, $a_R = 2\pi r B$ is the root surface density, r is the effective root radius, B is the root length density, k_r and $k_s = K_s/l$ are the root membrane permeability and the conductance associated with the radial flow within the soil to the nearest rootlet, respectively, and $l = 0.53/\sqrt{\pi B}$, the length scale characterizing the mean radial distance for the movement of water molecules from the bulk soil to the root surface within the rhizosphere (Vogel *et al*., 2013).

Formulated in this manner, the root water potential ψ_r is hydrostatically distributed (i.e. $\psi_r = \psi_{sb} - z_s$) assuming that the water storage and energy losses are negligible within the transporting roots (Lafolie *et al*., 1991; Siqueira *et al*., 2008). When compared with aboveground compartments, significantly larger hydraulic conductivity (Kavanagh *et al*., 1999) but smaller water storage capacity (Waring *et al*., 1979) in the rooting system suggests that this assumption may not be too restrictive for tree species. Independent model runs (not shown) also confirm the negligible effects of root water storage and resistance on both above- and belowground water dynamics. The coupling between the below- and aboveground plant systems is accomplished by imposing a continuous water potential from soil (ψ_s) to stem base (ψ_{sb}), and its resulting 'net' root water uptake ($\mathrm{RWU_{net}}$) supplied to the stem base can be expressed by the water balance for the bulk rooting system:

$$q_{p,sb} = \mathrm{RWU_{net}} = \left[\int_0^{L_R} (Q_r^+ + Q_r^-)\mathrm{d}z_s\right] \rho A_{soil} \quad \text{(Eqn 9)}$$

where $q_{p,sb}$ is the sap flow rate at the stem base, A_{soil} is the soil surface area covering the roots, and L_R is the rooting depth.

During daytime, water loss from leaves creates a significant water potential gradient from roots to leaves and induces water extraction throughout the rooting system (i.e. $Q_{r,day}^- = 0$ for all z_s) if the upper layers of the soil are not too dry and do not serve as competing sinks. However, the root water uptake at night from wet soil layers may be released back to dry soil layers or refills the xylem volume where PWS has been depleted by previous daytime transpiration. While the former mechanism is commonly termed 'hydraulic redistribution' and the amount of redistributed soil water through the

rooting system can be quantified by $\left|\int_0^{L_R} Q_r^- \mathrm{d}z_s\right| \rho A_{soil}$, the 'nocturnal refilling' to PWS is used to describe the later mechanism.

Leaf-level water balance

The water balance in the foliage is described elsewhere (Kumagai, 2001) but is modified to include a leaf-lamina resistance and is used as the upper boundary condition for water transport within the plant system. The leaf-level water balance is given as:

$$A_l(\Delta z_l)\left[C_l\frac{\partial\psi_l}{\partial t}\right] = -\left[q_{p,top} - F_e\right]$$
$$q_{p,top} = A_l\frac{(\psi_{p,top}-\psi_l)}{r_l}$$
$$F_e = A_l f_e m_v, \qquad \text{(Eqn 10)}$$

where A_l is leaf area, Δz_l is the effective leaf thickness, ψ_l is the leaf water potential, C_l is the hydraulic capacitance of the leaf, r_l is the leaf-lamina resistance, $q_{p,top}$ is the sap flux entering the leaf, F_e is the total crown transpiration flux, $\psi_{p,top}$ is the water potential at the distal conductive segment attached to the leaf, and f_e is the leaf-level transpiration rate, which can be converted to mass-based units using the molecular weight of water m_v and upscaled to F_e using leaf area A_l. C_l is assumed to be independent of ψ_l although this dependence can be incorporated if known.

The resistance to water flow through the leaf lamina is necessary because r_l may significantly contribute to whole-plant resistance which determines the leaf-level water status (Cruiziat *et al*., 2002; Taneda & Tateno, 2011) and in turn limits the response of the leaf-level gas exchange to drought stress. The effects of boundary layer conductance on leaf-level gas exchange are also included (Huang *et al*., 2015) so as to eliminate the use of vapor pressure deficit as a surrogate for actual evaporative demand (i.e. well-coupled leaf-to-atmosphere condition). As $F_{e,night}$ typically accounts for 10–30% of daily transpiration (Caird *et al*., 2007; Dawson *et al*., 2007; Novick *et al*., 2009), this water leakage from both guard cells and cuticle is also accounted for through a residual conductance (g_{res}) when night-time evaporative demand is finite. The leaf- gas exchange model utilizes a Fickian mass transfer across the laminar boundary layer attached to the leaf surface, which is then combined with the biochemical demand for CO_2 described by the Farquhar photosynthesis model for C_3 species (Farquhar *et al*., 1980). A leaf-level energy balance (Campbell & Norman, 1998) model and an optimal water-use strategy (i.e. maximizing the 'net' carbon gain at a given f_e) are used to determine variations in stomatal conductance (g_{s,CO_2}) and leaf-level assimilation rate (f_c) and f_e. The model description can be found elsewhere (Huang *et al*., 2015).

An optimality hypothesis for leaf-level gas exchange is equivalent to maximizing the objective function (or Hamiltonian):

$$h_a\left(g_{s,CO_2}\right) = f_c - \lambda f_e \quad \text{(Eqn 11)}$$

where the species-specific cost of water parameter λ is known as the marginal water-use efficiency (WUE) and measures the cost of water loss in carbon units. Mathematically, λ is the Lagrange multiplier for the unconstrained optimization problem and is approximately constant on time scales comparable to stomatal aperture fluctuations (Cowan & Farquhar, 1977; Katul *et al*., 2009, 2010). However, λ can gradually increase on a daily time-scale as a consequence of the reduction in soil water availability during a dry-down (Manzoni *et al*., 2013b). This continuing increase in λ ultimately results in complete stomatal closure. The linkage between λ and Ψ_l derived from a meta-analysis of *c*. 50 species (Manzoni *et al*., 2011) is adopted for the description of the increasing λ as drought progresses and is given by:

$$\lambda(\overline{\psi}_l) = \lambda^* \frac{c_a}{c_a^*} \exp\left[-\beta \overline{\psi}_l\right] \quad \text{(Eqn 12)}$$

(λ^*, the marginal WUE under well-watered soil conditions at a reference atmospheric CO
2 concentration $c_a^* = 400$ ppm.) $\overline{\Psi}_l$ is computed as an averaged $\Psi_l$over the previous 24-h period and represents a hydraulic signal that constrains the variation of stomatal aperture, and β is a species-specific sensitivity parameter. It should be emphasized that $\overline{\Psi}_l$ in Eqn 12 is not an instantaneous $\Psi_l$because the unconstrained optimization problem requires λ to vary on much longer time-scales than fluctuations in stomatal aperture, as noted in the text following Eqn 11. Because of this time integration of Ψ_l, a dynamic PWS also impacts g_{s,CO_2}, suggesting that a reduced soil water availability does not guarantee an immediate drop in $\overline{\Psi}_l$. In lieu of Ball–Berry (Ball *et al*., 1987) or Leuning (1995) semi-empirical models, the use of such an optimality hypothesis to maximize h_a reflects how the regulation of water loss through stomatal guard cells responds to water status at the leaf without invoking *ad hoc* correction functions (e.g. Tuzet *et al*., 2003) to 'externally' reduce maximum g_{s,CO_2} or f_e as deviations from well-watered soil conditions during dry-down. It also allows a direct coupling between the carbon and water economies of the leaf through $h_a$which must be positive to ensure optimality. To illustrate, the value of λ increases with decreasing $\overline{\Psi}_l$, leading to a gradual stomatal closure during a dry-down until a critical point (i.e. $\overline{\Psi}_{l,c}$) is reached, as shown in Fig. 2(b). Assuming that stomata *per se* operate only with a finite optimal 'net' carbon gain (i.e. $h_a > 0$ when $\lambda < \lambda_c$), the critical point can now be defined as λ_c, where the carbon gain is completely canceled out by the water cost in carbon units (Fig. 2c). This assumption may be plausible and ensures no more water loss (i.e. complete stomatal closure) when finite net carbon gain (i.e. $h_a > 0$) cannot be attained by any finite g_{s,CO_2} (inset in Fig. 2c). Before complete stomatal closure is reached, the duration of a finite g_{s,CO_2} (T_c) can then be tracked. Also, the total carbon uptake (C_{uptake}) that occurs while maintaining finite assimilation is given as:

$$C_{\text{uptake}} = \int_0^{T_e} f_c(g_{s,CO_2}(t))dt \quad \text{(Eqn 13)}$$

Thus, the species-specific λ–$\overline{\Psi}_l$ relation can accommodate a wide range of plant water-use strategies such as isohydric/anisohydric and is hereafter referred to as a 'leaf-level hydraulic signal curve'. Furthermore, the xylem water potential with respect to $\overline{\Psi}_{l,c}$ (i.e. P_c) is shown to be larger than P_{12} indicating that complete stomatal closure actually occurs before runaway cavitation (see Fig. 2a and the section 'Plant conducting tissues'). Hence, a coordination between stomatal closure and P_c arises naturally from the Hamiltonian to be maximized, which is one of the main novelties linking leaf-to-xylem here.

Model set-up

Eight scenarios (S1–S8) were constructed to explore the variations in environmental factors and plant traits (Table 2). To contrast the effects of plant attributes on the use of PWS, HR and C_{uptake} within T_e, the parameters C_p, g_{res}, leaf area index (LAI) and *H* are reduced in scenarios S2, S3, S7 and S8, relative to S1, while all other model parameters and environmental conditions are maintained the same. Using identical total root density and L_R, the root distribution shape is explored by a comparison between constant and power-law rooting profiles in S4 and S6, respectively. How site factors impact soil–plant water dynamics is explored through varying soil types (e.g. sandy clay loam in S4) and lower boundary conditions (e.g. constant water table in S5) and comparison with S1 (sandy soil with free drainage at the bottom of the soil column). The modeling approach is intended for a single tree but can be used for the whole stand/canopy when horizontal homogeneity is assumed for all soil–plant attributes across each compartment. While tree age can be accommodated by prescribed physiological, hydraulic and allometric attributes, the plant water-use strategy (i.e. isohydric or anisohydric) is not assumed and is embedded in the leaf-level hydraulic signal curve of Eqn 12. As the physiological, hydraulic and allometric attributes for each compartment are rarely available from a single experiment, a literature survey was conducted with a focus on coniferous species in general and pine plantation trees specifically to obtain consistent parameters (Supporting Information Methods S1). For all runs, the initial conditions are specified as near saturation in the plant vascular system and the soil column across all layers. The whole system is then allowed to drain for 12 h (i.e. one night's duration) only by gravitational forces without activating leaf-level gas exchange and $E_{c,night}$. With this initialization, the amount of water in the system is approximately identical for all scenarios except for the case of constant groundwater level (i.e. S5). Subsequently, the model calculations repeat with prescribed atmospheric variables on a periodic 24-h basis (Fig. S1.1) and that causes leaf-level gas exchange to operate. In the following sections, the general features of PWS usage and HR common to the scenarios are first presented in the Results section. The Discussion section then provides further elaboration of the one-to-one comparison across the scenarios so as to unfold the ways in which exogenous

environmental factors and endogenous plant attributes impact the spatio-temporal dynamics of water movement in the soil–plant system. Using a data set specifically collected from a *Pinus taeda* L. stand, reasonable agreement between the measured and modeled water usage in the plant and the soil during a 14-d dry-down is also shown in Methods S2.

Table 2. Eight scenarios (S1–S8) set up to explore the use of plant water storage (PWS)

	S1	S2	S3	S4	S5	S6	S7	S8
H (m)	20	20	20	20	20	20	20	10
C_p (kg m^{-3} MPa^{-1})[a]	L	S	L	L	L	L	L	L
LAI (m^2 m^{-2})	6	6	6	6	6	6	4	6
g_{res} (mol m^{-2} s^{-1})	0.04	0.04	0.02	0.04	0.04	0.04	0.04	0.04
Lower boundary condition[b]	FD	FD	FD	FD	WT	FD	FD	FD
Root distribution[c]	U	U	U	U	U	PW	U	U
Soil type	Sand	Sand	Sand	Sandy clay loam	Sand	Sandy clay loam	Sand	Sand

H, tree height; C_p, specific hydraulic capacitance; g_{res}, residual conductance accounting for water leakage through guard cells and cuticle overnight; LAI, leaf area index.
[a]Two plant hydraulic capacitances: larger (L) and smaller (S) C_p values (see Supporting Information Methods S1).
[b]Two lower boundary conditions for the soil column: free drainage (FD) and water table (WT) set at 2 m depth below the soil surface.
[c]Two vertical root distributions: uniform (U) and power-law (PW) rooting profiles. Note that the power-law reduction function provides a more realistic description for coniferous species (Jackson *et al*., 1996; Finér *et al*., 1997; Andersson, 2005).

Results

General features of the modeled PWS usage

Using S1 as an example, Fig. 3(a) shows the typical diurnal pattern of F_e and $q_{p,sb}$ along with the modeled time delay between their peaks attributable to PWS. The computed delay is *c*. 1.5 h and is well within the range of 0.1–2.5 h reported elsewhere (Goldstein *et al*., 1998; Phillips *et al*., 2003;

Bohrer *et al*., 2005). The daily PWS consumed can be computed by integrating the differences between F_e and $q_{p,sb}$ when $F_e \geq q_{p,sb}$. Fig. 3(b) shows a larger diurnal variation in predicted θ_p near the tree crown, suggesting that the use of PWS can be primarily attributed to water depletion from xylem tissues closer to the transpiring sites. *In situ*experiments (Schulze *et al*., 1985; Loustau *et al*., 1996) on coniferous species also reported a pattern consistent with the modeled results presented here. As the ascent of water from the soil to the tree crown may require a few days to replenish the distal part of the conducting tissues (Granier, 1987; Dye *et al*., 1996; Zang *et al*., 1996), this finding is perhaps not surprising, especially as the water stored in the upper parts of the plant can be immediately transpired by leaves. The modeled daily PWS usage normalized by daily F_e and the modeled 'actual' PWS usage without normalization are presented in Fig. 4(a) and (b), respectively. When soil water status cannot be recovered (i.e. there is continuing loss of soil water through transpiration and drainage) during the dry-down, the increasing reliance on PWS with respect to F_e is inevitable. This finding appears to be consistent with sap flow measurements reported elsewhere (Loustau *et al*., 1996; Phillips *et al*., 2003). When the soil water availability is not limited as a result of the presence of a shallow groundwater table (i.e. S5), the water depleted by F_e in the soil column and plant xylem tissues can be completely recovered to its previous state within a single diurnal cycle. This explains why the use of PWS as well as HR (see Fig. 6(a,b) and section 'General features of the modeled HR') for S5 remains constant during the dry-down. The modeled average daily PWS usage across all scenarios ranges from 1.1% to 23.3% when normalized by daily F_e and from 0.07 to 1.61 kg m $^{-2}$ (ground) d $^{-1}$ without normalization.

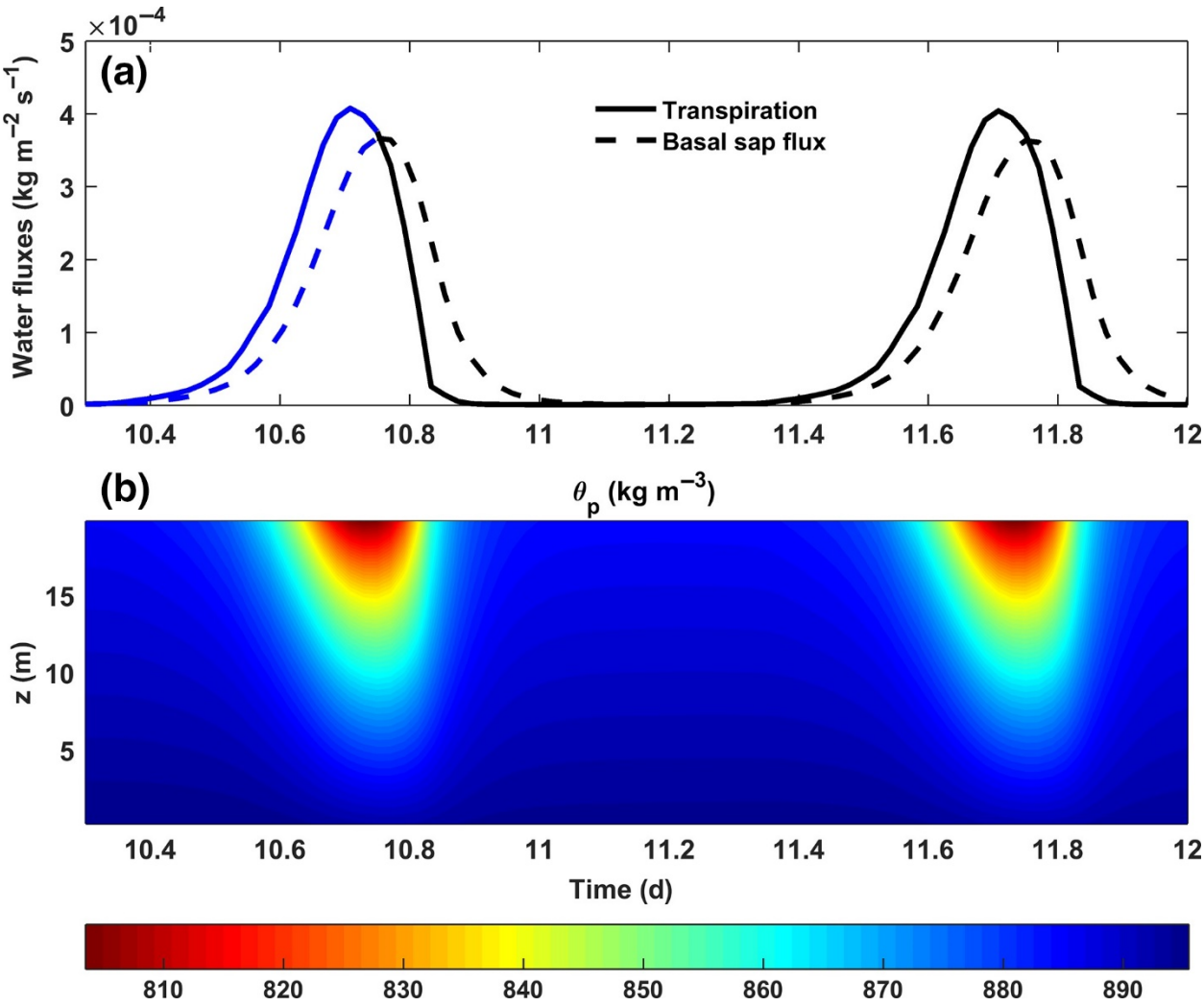

Figure 3. (a) Modeled transpiration rate (F_e) and basal sap flux ($q_{p,sb}$) during a single dry-down period commencing with near saturation at t = 0 d on a per unit ground area basis. (b) Modeled profile of plant xylem water content (θ_p) with units of kg m^{-3} for S1 (see Table 3 for model set-up). Note that daily plant water storage (PWS) usage is determined from the area bounded by the solid and dashed blue lines.

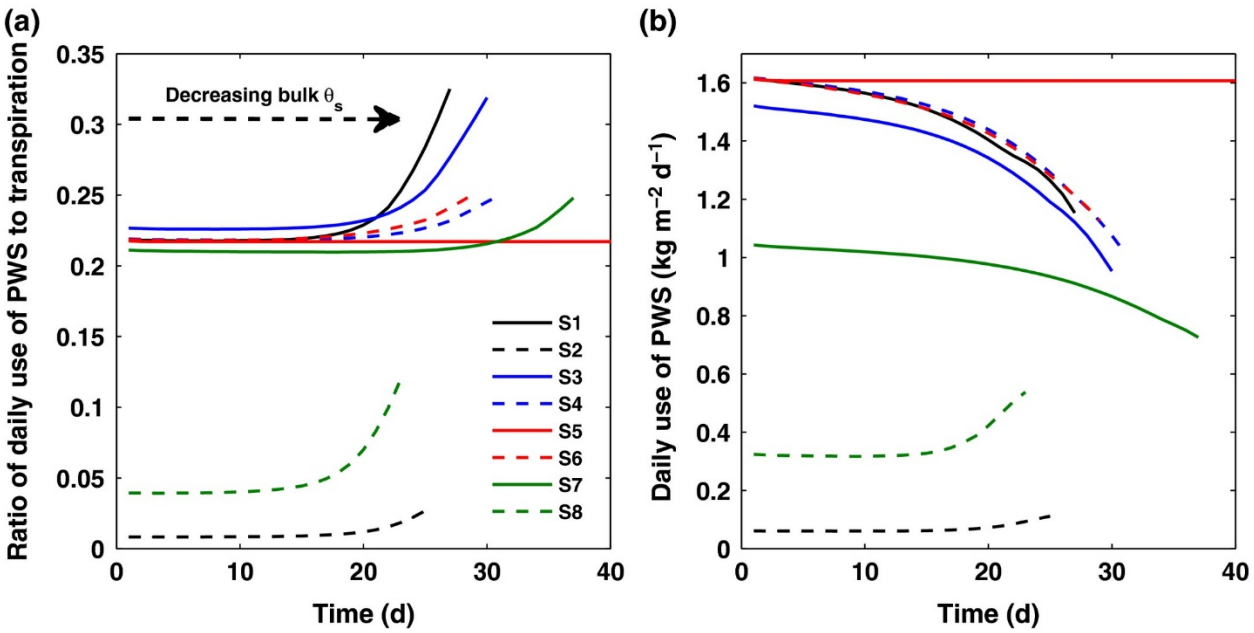

Figure 4. Modeled daily use of (a) plant water storage (PWS) normalized by daily transpiration and (b) PWS on a per unit ground area basis for the eight scenarios (see Table 3 for the model set-up).

General features of the modeled HR

The modeled diurnal variations in θ_s and Q_r profiles across L_R are shown in Fig. 5(a) and (b) respectively for S6, which is the largest HR across all eight scenarios. Although the overall θ_s decreases with progressively drying soil conditions, HR can partially refill θ_s in the upper layers when a finite ψ_s gradient across L_R is maintained and F_c recedes to a minimum at night. In the presence of PWS and $F_{c,night}$, daily HR can be computed using the total Q_r^- across each layer on a daily basis. For all runs, modeled daily HR normalized by daily F_c and modeled daily HR without normalization are shown in Fig. 6(a) and (b), respectively. With the exception of S5, a bell-shaped HR cycle during the dry-down process emerges and reaches a maximum value when the largest ψ_s vertical gradient across L_R occurs. In the early phases of the dry-down, θ_s and ψ_s in the upper soil layers are reduced rapidly when compared with θ_s in the deeper layers, thereby generating a continuously increasing ψ_s gradient across L_R, resulting in an increasing HR. After the ψ_s gradient reaches a maximum across L_R, the water located within the upper soil layers becomes difficult to extract by roots and most of the contribution from Q_r^+ to F_c is shifted to deeper soil layers. As a result, the $\psi_s$gradient is gradually 'evened out' resulting in a decreasing trend in HR. This dynamic drying process across the soil layers explains the bell-shaped HR cycle reported in the literature (Meinzer *et al*., 2004; Warren *et al*., 2005; Scholz *et al*., 2008; Prieto *et al*., 2010). The modeled average and maximum magnitudes of HR across all scenarios are, respectively, in the range of 6.3–16.7% and 0.63–22.9% when normalized by daily F_c, and in the range of 0.43–1.08 and 0.47–1.56 kg m^{-2} d^{-1} without normalization, a result more comparable to previous empirical estimates of HR (e.g. 20% of F_c and 0.42 kg m^{-2} d^{-1} on average with

the maximum of 1.1 kg m^{-2} d^{-1} for loblolly pine (*Pinus taeda* L.)) summarized elsewhere (Neumann & Cardon, 2012). While previous modeling studies tended to provide higher HR estimates (Neumann & Cardon, 2012), the proposed approach here ameliorates such high modeled HR by accounting for PWS changes and $F_{c,night}$ (i.e. g_{res}) which increase the residual water potential gradient at night ($\Delta\psi_{p,night}$) and reduce the magnitude of HR.

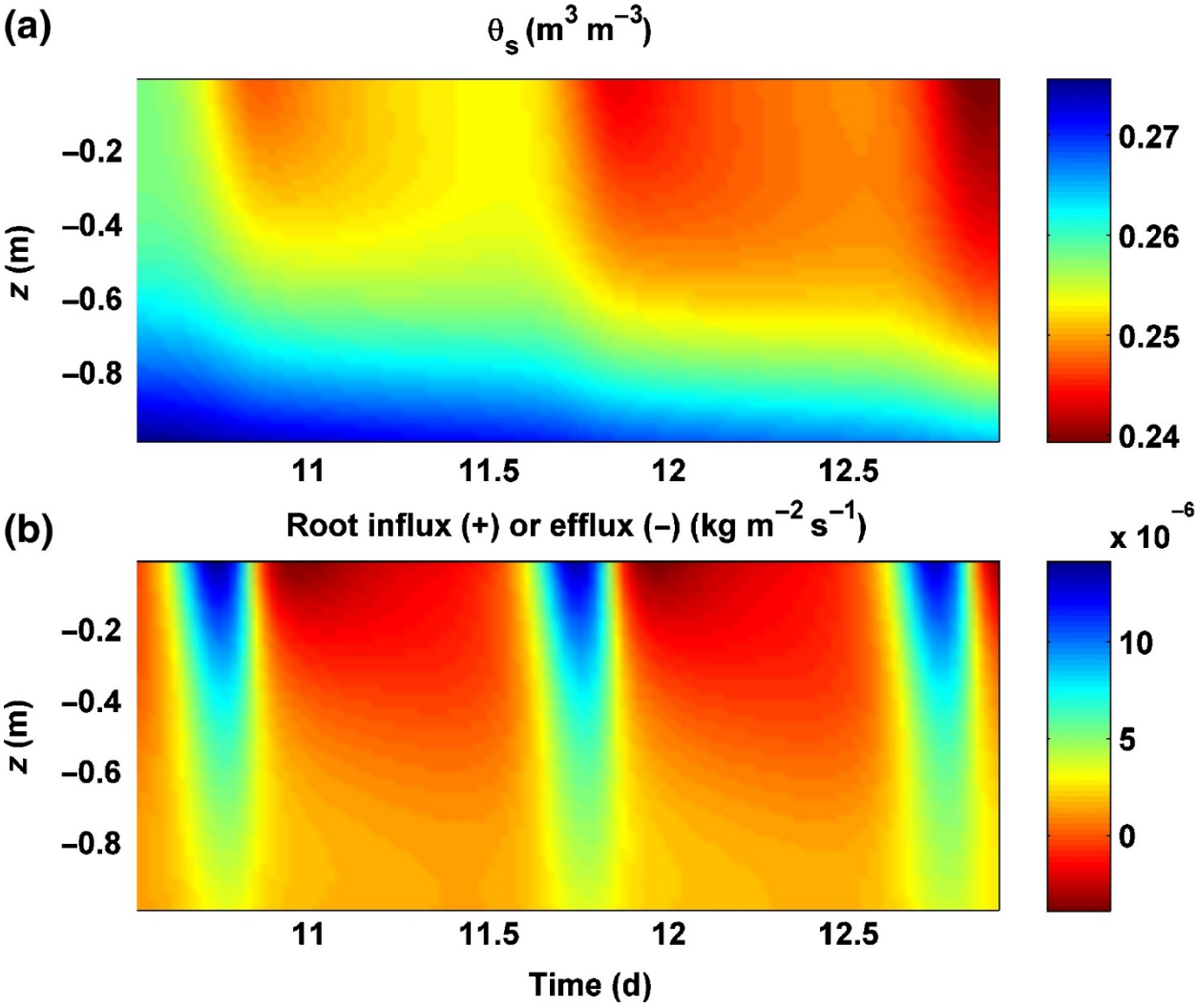

Figure 5. Modeled profiles of (a) soil water content (θ_s) and (b) root water influx (Q_r^+) or efflux (Q_r^-) on a per unit ground area basis for S6 (see Table 3 for model set-up).

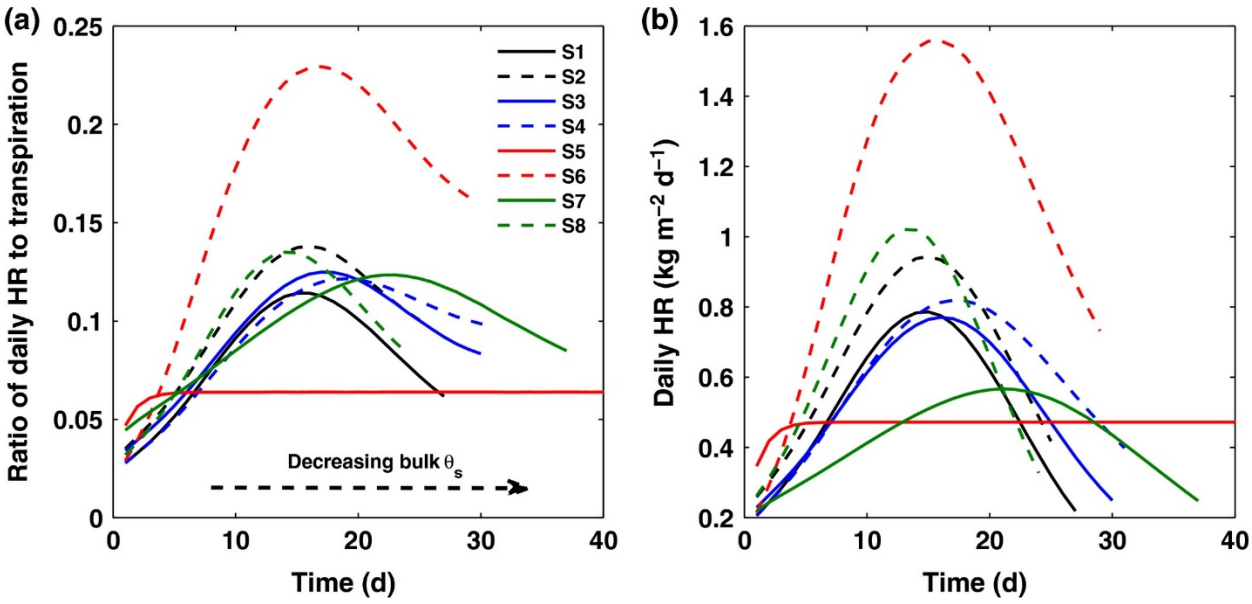

Figure 6. Modeled daily hydraulic redistribution (HR) (a) normalized by daily transpiration and (b) on a per unit ground area basis for the eight scenarios (see Table 3 for model set-up).

Discussion

Model analysis for PWS usage

The modeled use of PWS tends to diminish under two conditions: a smaller $C_{p,total}$caused by reducing C_p or *H* and a smaller F_e caused by a reduced g_{res} or LAI. PWS usage is interpreted as the integrated water flux gradient along the transpiration stream from stem base to leaf lamina. Hence, reductions in F_e with a smaller g_{res}or LAI (i.e. S3 and S7) promotes a smaller water flux gradient that then suppresses the use of PWS. Daytime F_e and $F_{e,night}$ are reduced by a smaller g_{res}. As expected, a smaller C_p or *H* (i.e. S2 and S8) provides less 'available' water space for F_e given that $C_{p,total}$ represents an effective measure of whole-plant water storage. As the contribution of PWS to F_e is reduced by a smaller $C_{p,total}$, the water flux gradient is further reduced, resulting in lower use of PWS for S2 and S8. The increasing trend in PWS usage with increasing tree size appears consistent with field experiments conducted for different tree sizes across different species or within the same species (Goldstein *et al.*, 1998; Phillips *et al.*, 2003). Vertical heterogeneity in root distributions may have only a minor impact on the use of PWS but a potentially significant impact on RWU_{net} and F_e. The comparison for different root distributions (i.e. S4 and S6) suggests that less PWS is used for the case of a power-law root distribution (i.e. S6). Hence, RWU_{net} (i.e. $q_{p,sb}$) is reduced if the majority of root density is concentrated within the upper dry soil layers. As a consequence of the reduction in RWU_{net}, daytime F_e appears to decrease as well. As a result, the more rapid reduction in daytime F_e when compared with RWU_{net}can be used to explain the lower PWS usage in S6 when compared with S4. Taken together, these findings suggest that greater use of PWS implies a more efficient RWU_{net} to

mitigate against drought conditions (i.e. maintain highest leaf photosynthesis at a given f_e), especially when roots are competing with drainage losses (see section 'Combined effects of PWS and HR on C_{uptake} and T_c'). The modeled results also indicate that more PWS usage occurs in less sandy soils (i.e. S4) or where the groundwater level is shallower (i.e. S5). In contrast to the sandier soil type, higher soil water availability conditions can be maintained in finer-textured soil (i.e. less conductive) even though drainage is allowed. It is for this reason that the more rapid increase in F_e than RWU_{net} generates greater PWS usage for S4. When a shallow groundwater table is externally imposed on the soil system, the diurnal recovery of soil water status through HR or Darcian redistribution explains why the use of PWS for S5 can be maintained constant.

Model analysis for HR

In Fig. 7, the partitioning between night-time HR and RWU_{net} (i.e. nocturnal refilling) normalized by total root water influx at night over the dry-down period is illustrated. This figure shows how increases in nocturnal refilling suppress HR across all scenarios. HR is impacted by $C_{p,total}$ and F_e in opposite ways. The above-ground sink strength can be reduced by a smaller $C_{p,total}$ (i.e. S2 and S8) or F_e (i.e. S3 and S7) which potentially enhance HR differently as drought progresses. When compared with S1, the ψ_s gradient driving HR for S2 and S8 is approximately the same, given a similar daytime F_e for these three scenarios. However, the $\psi_s$gradient for S1 is compensated for by a larger above-ground competing sink strength (i.e. PWS refilling) that directly suppresses HR. It can be stated that the soil water drawn by the rooting system at night in S1 contributes more to recharging θ_p depleted by previous daytime F_e but not θ_s in the drier and shallower soil layers. When $\Delta\psi_{p,night}$ induced by $F_{e,night}$ is ruled out, a pattern similar to that reported elsewhere (Hultine *et al*., 2003) emerges. Although the aboveground competing sink strength for S3 and S7 is smaller than for S1, their ψ_s gradients driving HR cannot rapidly develop because of a reduced daytime $F_e$but can be retained with a longer duration when compared with S1. It is for this reason that a wider but shallower bell-shaped HR cycle is formed for cases S3 and S7, implying a larger amount of HR in total but a lower intensity of HR during the dry-down process. If night-time evaporative demand (averaged overnight vapor pressure deficit is 0.07 kPa computed from the measured atmospheric variables shown in Fig. S1.1; not g_{res}) is set to zero to suppress only $F_{e,night}$, an immediate increase in the intensity of HR is predicted (not shown here), consistent with a number of experiments manipulating $F_{e,night}$ (Hultine *et al*., 2003; Scholz *et al*., 2008; Howard *et al*., 2009; Prieto *et al*., 2010). Over a single dry-down, the increase in modeled HR with zero $F_{e,night}$ is *c*. 10% across all scenarios. However, the model calculations suggest that the reduction in HR attributable to the presence of $F_{e,night}$ may be less significant when compared with larger $C_{p,total}$ (i.e. >22% reduction in HR). Among the many plant attributes affecting HR, the variation in root distribution can directly alter the pattern of the ψ_s gradient along L_R even when the above-ground competing sink strength is maintained the

same. If the root density is concentrated in the upper soil layers as in S6, representing coniferous species (Jackson *et al*., 1996; Finér *et al*., 1997; Andersson, 2005), significant daytime depletion of soil water in the upper layers (Fig. 5) produces a much larger ψ_s gradient. This large ψ_s gradient across soil layers increases the magnitude of HR when compared with uniform or linear root distributions. A larger HR corresponding to a vertically asymmetric root distribution has been found in other experiments and model calculations (Hultine *et al*., 2003; Scholz *et al*., 2008; Siqueira *et al*., 2008; Volpe *et al*., 2013), lending some support to the model results presented here.

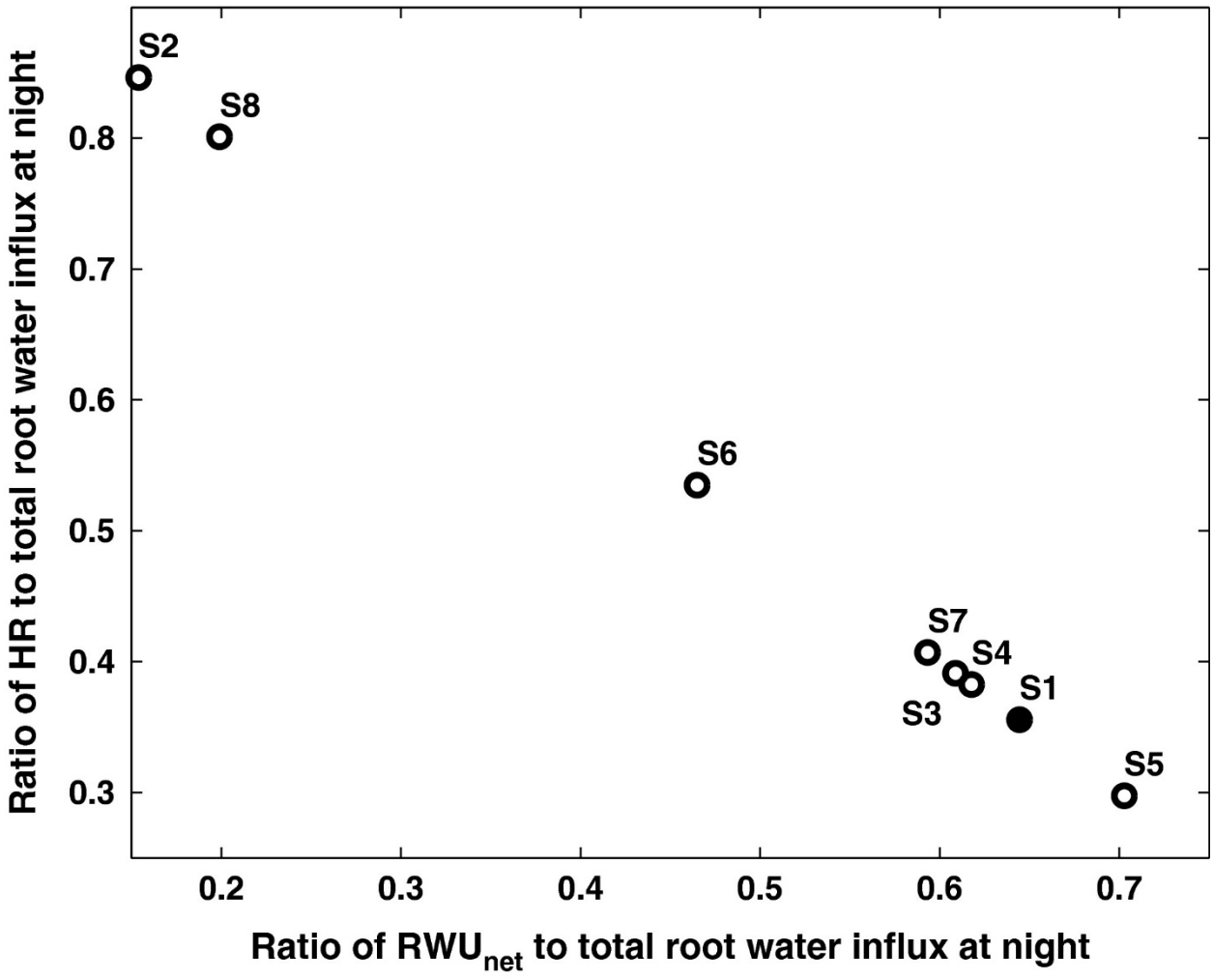

Figure 7. The partitioning between night-time hydraulic redistribution (HR) and net root water uptake (RWU_{net}) normalized by total root water influx at night over a single dry-down period.

Regarding soil texture, the comparison between S1 and S4 suggests that sandy soils result in a smaller intensity and duration (i.e. frequency) of HR (Yoder & Nowak, 1999; Wang *et al*., 2009) compared with their clay counterparts. Rapid drainage in coarse-textured soils impedes the development of the ψ_s gradient required for the onset of HR (Burgess *et al*., 2000; Scholz *et al*., 2008). Moreover, the loss of soil–root contact (i.e. a larger *l* is expected here) at low θ_s can further diminish the ability of

roots to exude water (i.e. Q_r^-) even when the Ψ_s gradient is well developed (Wang *et al*., 2009). As *l* is held constant here with a pre-specified *B*for any θ_s condition, this reduction in Q_r^- is only possible through reductions in $K_s$and *k* (see Eqn 8). As discussed earlier (see section 'General features of the modeled PWS usage'), HR at night can be maintained constant for the case of groundwater level adjacent to L_R (i.e. S5) given a constant Ψ_s gradient generated by daytime F_c. This finding also implies that the magnitude of HR with a shallow groundwater level mainly depends on the magnitude of the previous daytime $F_c$when belowground conditions (i.e. soil type, groundwater level and root attributes) are not varying. However, the Ψ_s gradient driving HR in this case does not accumulate with progressively drying soil conditions resulting in a smaller HR magnitude.

Interestingly, when all the factors that potentially impact the magnitude of HR are combined, plausible explanations can be offered for the conflicting results of two empirical studies on HR with rooting system near or in contact with a groundwater table: sugar maple (*Acer saccharum*) with significant HR (Dawson, 1993; Emerman & Dawson, 1996) and three desert phreatophytic plants with insignificant HR (Hultine *et al*., 2003). Although $F_{c,night}$ for sugar maple is among the largest reported from a literature survey (Dawson *et al*., 2007), the Ψ_s gradient along L_R is not reduced by $\Delta\Psi_{p,night}$ when deeper roots are in contact with groundwater. Thus, the significant Ψ_s gradient across L_R, which was developed by a large daytime F_c (Dawson *et al*., 2007), fine-textured soil type (i.e. silt loam) and asymmetric root distribution, can intensify the magnitude of HR in this case. However, the Ψ_s gradient for the three desert phreatophytes may be lacking as a consequence of the combined effects of sandy soil (up to 84% sand) and small daytime F_c, thereby suppressing the occurrence of HR.

Combined effects of PWS and HR on C_{uptake} and T_c

It can be conjectured that a larger T_c improves the capabilities of a plant to resist drought stress and enhance C_{uptake} over a longer period. T_c varies with different scenarios because the temporal variation in $\overline{\Psi_l}$ dictating T_c is impacted by the combined effects of F_c and RWU_{net} as well as PWS and HR. Thus, how RWU_{net}varies across different scenarios can be used to explore how T_c and C_{uptake} are affected by PWS and HR. The modeled C_{uptake} shown in Fig. 8(a) features an increasing trend with respect to T_c when leaf-level physiological parameters remain the same across the scenarios. T_c during a dry-down period is used as an indicator of the extended use of soil water to sustain C_{uptake} for each of the eight scenarios. The coordinated relationship between stomatal behavior and plant hydraulics is also illustrated in Fig. 9, showing the modeled time-course of $g_{s,CO_2}$and water potential in each compartment as well as the corresponding $\overline{\Psi_l}$. The g_{s,CO_2} decreases with decreasing $\overline{\Psi_l}$ (not bulk Ψ_s) because the cost of water in carbon units (i.e. λ) increases as specified by the hydraulic signal curve. Moreover, the rapid reduction in Ψ_s compared with the smoothly varying $\overline{\Psi_l}$ indicates how PWS impacts this hydraulic signal and subsequent leaf-level gas exchange.

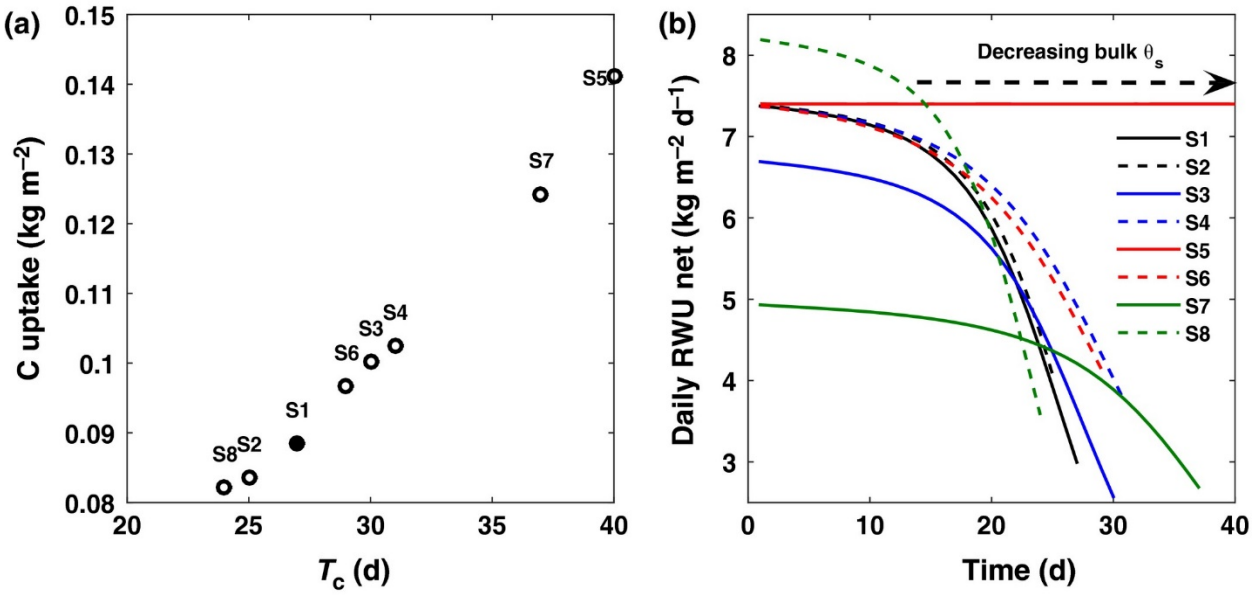

Figure 8. (a) Modeled total carbon uptake (C_{uptake}) on a per unit leaf area basis in relation to the duration of a finite g_s,CO_2 (T_c) for each scenario. (b) Modeled daily net root water uptake (RWU_{net}) on a per unit ground area basis for the eight scenarios (see Table 3for model set-up). Note that T_c for S5 is indefinite and is terminated at 40 d for reference.

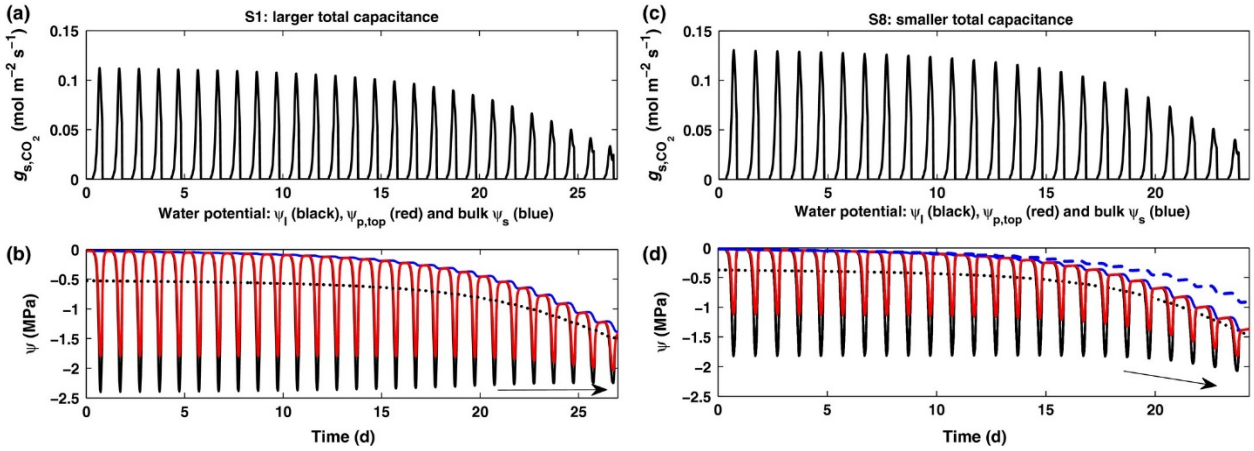

Figure 9. (a) Modeled stomatal conductance (g_{s,CO_2}) and (b) modeled water potential in each compartment for S1. (c) Modeled g_{s,CO_2} and (d) modeled water potential in each compartment for S8. Note that black solid, black dashed, red solid and blue solid lines are used to represent leaf water potential (ψ_l), 24 h averaged leaf water potential ($\overline{\psi}_l$), distal xylem water potential ($\psi_{p,top}$) and bulk soil water potential (ψ_s) across rooting depth (L_R), respectively. The bulk ψ_s for S1 (blue dashed line) is also included in (d) for reference. The T_c values for S1 and S8 are, respectively, 27 and 23 d (i.e. *x*-axis range for each scenario).

Fig. 8(b) shows that daily RWU_{net} decreases with decreasing bulk θ_s except for S5. A shallow groundwater level can support a constant daily RWU_{net} and F_c, preventing $\overline{\psi}_l$ from being reduced to $\overline{\psi}_{l,c}$. This explains why T_c is indefinite unless this ideal balance between demand and supply is discontinued. To contrast the effects of atmospheric demand (i.e. F_c) on T_c when $C_{p,total}$ remains the same, a larger T_c is predicted by reductions in F_c with a reduced g_{res} (i.e. S3) or LAI (i.e. S7) in

comparison to S1. Apparently, RWU_{net} needed for E_c in such cases is reduced. Wetter soil conditions and a larger $\overline{\Psi_l}$ here can be maintained for a longer period to support leaf-level gas exchange. When $C_{p,total}$ is reduced by using a smaller C_p(i.e. S2) or *H* (i.e. S8) compared with S1, a rapid reduction in $\overline{\Psi_l}$ is found to diminish T_c in both cases. Although the total HR and RWU_{net} in these two cases are larger than in S1, Ψ_s still cannot be maintained in a wetter conditions when a larger amount of RWU_{net} is required as a consequence of a lack of available PWS. Adopting the two end members for total hydraulic capacitance (i.e. S1 and S8) as examples (Fig. 9), larger PWS to compensate for the decline in bulk θ_s and $\Psi_l$enhances T_c (and C_{uptake}) as drought progresses, thereby delaying the incipient reduction in $\overline{\Psi_l}$.

Examining the model results for S4 and S6, it is evident that the magnitude of RWU_{net} is suppressed by the case of root density concentrated in the upper soil layers (i.e. S6). Unlike previous $C_{p,total}$ comparisons, $\overline{\Psi_l}$ can be less negative (i.e. larger T_c) as a result of a larger RWU_{net} provided that $C_{p,total}$ for the two cases differing in root distributions is the same. Again, a larger HR promoted by asymmetric root distribution overnight cannot directly contribute to RWU_{net} mainly occurring during the daytime. Regarding soil texture, more RWU_{net} can be supported by less sandy soil (i.e. S4). Similar to the comparison for the two end members of root distribution, T_c is increased by a larger RWU_{net} if $C_{p,total}$ is held constant. Hence, finer-textured soil prevents a rapid decline in $\overline{\Psi_l}$ and yields larger T_c.

To sum up, routing available soil water into PWS instead of HR can be more advantageous when drought progresses and soil water availability is the main limiting factor even in the absence of competing species (Methods S3). However, the significance of HR associated with enhancement of nutrient uptake through maintaining soil–root contact, rendering water to neighboring species and maintaining microbial activities cannot be overlooked (Prieto *et al*., 2012). Despite all the simplifications made in the proposed modeling approach, the framework here can serve as a 'hypothesis generator' to assess how exogenous environmental conditions and endogenous soil–root–stem–leaf hydraulic and eco-physiological properties shape plant responses to droughts. Testing such hypotheses requires coordinated field and laboratory experiments that measure water movement in all compartments of the soil–plant system.

Acknowledgements

Support from the National Science Foundation (NSF-CBET-103347, NSF-EAR-1344703 and NSF-DGE-1068871), the US Department of Energy (DOE) through the Office of Biological and Environmental Research (BER) Terrestrial Carbon Processes (TCP) program (DE-SC0006967 and DE-SC0011461), and the Nicholas School of the Environment at Duke University Seed Grant Initiative is acknowledged.

References

Andersson F. 2005. *Coniferous forests*, *vol. 6*. Amsterdam, the Netherlands: Elsevier.

Aumann C, Ford E. 2002. Modeling tree water flow as an unsaturated flow through a porous medium. *Journal of Theoretical Biology* **219**, 415–429.

Ball JT, Woodrow IE, Berry JA. 1987. A model predicting stomatal conductance and its contribution to the control of photosynthesis under different environmental conditions. In: Biggins I, ed. *Progress in photosynthesis research*, *vol. 4*. Dordrecht, the Netherlands: Martinus Nijhoff, Springer, 221–224.

Bohrer G, Mourad H, Laursen T, Drewry D, Avissar R, Poggi D, Oren R, Katul G. 2005. Finite element tree crown hydrodynamics model (FETCH) using porous media flow within branching elements: a new representation of tree hydrodynamics. *Water Resources Research* **41**, W11404.

Bond BJ, Kavanagh KL. 1999. Stomatal behavior of four woody species in relation to leaf specific hydraulic conductance and threshold water potential. *Tree Physiology* **19**, 503–510.

Bonetti S, Manoli G, Domec JC, Putti M, Marani M, Katul G. 2015. The influence of water table depth and the free atmospheric state on convective rainfall predisposition. *Water Resources Research* **51**, 2283–2297.

Brodribb T, Cochard H. 2009. Hydraulic failure defines the recovery and point of death in water-stressed conifers. *Plant Physiology* **149**, 575–584.

Brough D, Jones H, Grace J. 1986. Diurnal changes in water content of the stems of apple trees, as influenced by irrigation. *Plant, Cell & Environment* **9**, 1–7.

Burgess SS, Pate JS, Adams MA, Dawson TE. 2000. Seasonal water acquisition and redistribution in the Australian woody phreatophyte,*Banksia prionotes. Annals of Botany* **85**, 215–224.

Caird MA, Richards JH, Donovan LA. 2007. Nighttime stomatal conductance and transpiration in C_3 and C_4 plants. *Plant Physiology***143**, 4–10.

Campbell GS, Norman J. 1998. *An introduction to environmental biophysics*. New York, NY, USA: Springer.

Chuang Y, Oren R, Bertozzi A, Phillips N, Katul G. 2006. The porous media model for the hydraulic system of a conifer tree: linking sap flux data to transpiration rate. *Ecological Modelling* **191**, 447–468.

Clapp R, Hornberger G. 1978. Empirical equations for some soil hydraulic properties. *Water Resources Research* **14**, 601–604.

Cowan I, Farquhar G. 1977. Stomatal function in relation to leaf metabolism and environment. In: Jennings DH, ed. *Symposia of the society for experimental biology*, *vol. 31*. Cambridge, UK: Cambridge University Press, 471–505.

Cruiziat P, Cochard H, Améglio T. 2002. Hydraulic architecture of trees: main concepts and results. *Annals of Forest Science* **59**, 723–752.

Dawson TE. 1993. Hydraulic lift and water use by plants: implications for water balance, performance and plant–plant interactions. *Oecologia* **95**, 565–574.
Dawson TE, Burgess SSO, Tu KP, Oliveira RS, Santiago LS, Fisher JB, Simonin KA, Ambrose AR. 2007. Nighttime transpiration in woody plants from contrasting ecosystems. *Tree Physiology* **27**, 561–575.
Domec J, Gartner B. 2001. Cavitation and water storage capacity in bole xylem segments of mature and young Douglas-fir trees. *Trees***15**, 204–214.
Domec J, King JS, Noormets A, Treasure E, Gavazzi M, Sun G, McNulty S. 2010. Hydraulic redistribution of soil water by roots affects wholestand evapotranspiration and net ecosystem carbon exchange. *New Phytologist* **187**, 171–183.
Dye P, Soko S, Poulter A. 1996. Evaluation of the heat pulse velocity method for measuring sap flow in *Pinus patula*. *Journal of Experimental Botany* **47**, 975–981.
Edwards W, Jarvis P, Landsberg J, Talbot H. 1986. A dynamic model for studying flow of water in single trees. *Tree Physiology* **1**, 309–324.
Emerman SH, Dawson TE. 1996. Hydraulic lift and its influence on the water content of the rhizosphere: an example from sugar maple, *Acer saccharum*. *Oecologia* **108**, 273–278.
Farquhar GD, von Caemmerer S, Berry JA. 1980. A biochemical model of photosynthetic CO 2 assimilation in leaves of C_3 species. *Planta* **149**, 78–90.
Finér L, Messier C, De Grandpré L. 1997. Fine-root dynamics in mixed boreal conifer-broad-leafed forest stands at different successional stages after fire. *Canadian Journal of Forest Research* **27**, 304–314.
Früh T, Kurth W. 1999. The hydraulic system of trees: theoretical framework and numerical simulation. *Journal of Theoretical Biology***201**, 251–270.
Goldstein G, Andrade J, Meinzer F, Holbrook N, Cavelier J, Jackson P, Celis A. 1998. Stem water storage and diurnal patterns of water use in tropical forest canopy trees. *Plant, Cell & Environment* **21**, 397–406.
Granier A. 1987. Evaluation of transpiration in a Douglas-fir stand by means of sap flow measurements. *Tree Physiology* **3**, 309–320.
Hentschel R, Bittner S, Janott M, Biernath C, Holst J, Ferrio JP, Gessler A, Priesack E. 2013. Simulation of stand transpiration based on a xylem water flow model for individual trees. *Agricultural and Forest Meteorology* **182**, 31–42.
Howard AR, Van Iersel MW, Richards JH, Donovan LA. 2009. Nighttime transpiration can decrease hydraulic redistribution. *Plant, Cell & Environment* **32**, 1060–1070.
Huang CW, Chu CR, Hsieh CI, Palmroth S, Katul GG. 2015. Wind-induced leaf transpiration. *Advances in Water Resources* **86**, 240–255.
Hultine K, Williams D, Burgess S, Keefer T. 2003. Contrasting patterns of hydraulic redistribution in three desert phreatophytes. *Oecologia* **135**, 167–175.
Jackson R, Canadell J, Ehleringer J, Mooney H, Sala O, Schulze E. 1996. A global analysis of root distributions for terrestrial biomes. *Oecologia* **108**, 389–411.

Katul GG, Manzoni S, Palmroth S, Oren R. 2010. A stomatal optimization theory to describe the effects of atmospheric CO_2 on leaf photosynthesis and transpiration. *Annals of Botany* **105**, 431–442.

Katul GG, Palmroth S, Oren R. 2009. Leaf stomatal responses to vapour pressure deficit under current and CO_2-enriched atmosphere explained by the economics of gas exchange. *Plant, Cell & Environment* **32**, 968–979.

Kavanagh K, Bond B, Aitken S, Gartner B, Knowe S. 1999. Shoot and root vulnerability to xylem cavitation in four populations of Douglas-fir seedlings. *Tree Physiology* **19**, 31–37.

Konrad W, Roth-Nebelsick A. 2003. The dynamics of gas bubbles in conduits of vascular plants and implications for embolism repair. *Journal of Theoretical Biology* **224**, 43–61.

Kumagai T. 2001. Modeling water transportation and storage in sapwood-model development and validation. *Agricultural and Forest Meteorology* **109**, 105–115.

Lafolie F, Bruckler L, Tardieu F. 1991. Modeling root water potential and soil–root water transport: I. Model presentation. *Soil Science Society of America Journal* **55**, 1203–1212.

Leuning R. 1995. A critical appraisal of a combined stomatal-photosynthesis model for C_3 plants. *Plant, Cell & Environment* **18**, 339–355.

Loustau D, Berbigier P, Roumagnac P, Arruda-Pacheco C, David J, Ferreira M, Pereira J, Tavares R. 1996. Transpiration of a 64-year-old maritime pine stand in portugal. *Oecologia* **107**, 33–42.

Maherali H, DeLucia E. 2001. Influence of climate-driven shifts in biomass allocation on water transport and storage in ponderosa pine. *Oecologia* **129**, 481–491.

Manoli G, Bonetti S, Domec JC, Putti M, Katul G, Marani M. 2014. Tree root systems competing for soil moisture in a 3D soil–plant model. *Advances in Water Resources* **66**, 32–42.

Manzoni S, Katul G, Porporato A. 2014. A dynamical system perspective on plant hydraulic failure. *Water Resources Research* **50**, 5170–5183.

Manzoni S, Vico G, Katul G, Palmroth S, Jackson RB, Porporato A. 2013a. Hydraulic limits on maximum plant transpiration and the emergence of the safety–efficiency trade-off. *New Phytologist* **198**, 169–178.

Manzoni S, Vico G, Palmroth S, Porporato A, Katul G. 2013b. Optimization of stomatal conductance for maximum carbon gain under dynamic soil moisture. *Advances in Water Resources* **62**, 90–105.

Manzoni S, Vico G, Porporato A, Katul G. 2013c. Biological constraints on water transport in the soil–plant-atmosphere system. *Advances in Water Resources* **51**, 292–304.

Manzoni S, Vico G, Katul G, Fay PA, Polley W, Palmroth S, Porporato A. 2011. Optimizing stomatal conductance for maximum carbon gain under water stress: a meta analysis across plant functional types and climates. *Functional Ecology* **25**, 456–467.

McDowell N, Pockman W, Allen C, Breshears D, Cobb N, Kolb T, Plaut J, Sperry J, West A, Williams D. 2008. Mechanisms of plant survival and mortality during drought: why do some plants survive while others succumb to drought? *New Phytologist* **178**, 719–739.

Meinzer F, Brooks J, Bucci S, Goldstein G, Scholz F, Warren J. 2004. Converging patterns of uptake and hydraulic redistribution of soil water in contrasting woody vegetation types. *Tree Physiology* **24**, 919–928.

Neumann R, Cardon Z. 2012. The magnitude of hydraulic redistribution by plant roots: a review and synthesis of empirical and modeling studies. *New Phytologist* **194**, 337–352.

Novick KA, Oren R, Stoy PC, Siqueira MBS, Katul GG. 2009. Nocturnal evapotranspiration in eddy-covariance records from three co-located ecosystems in the Southeastern U.S.: implications for annual fluxes. *Agricultural and Forest Meteorology* **149**, 1491–1504.

Parolari AJ, Katul GG, Porporato A. 2014. An ecohydrological perspective on drought induced forest mortality. *Journal of Geophysical Research: Biogeosciences* **119**, 965–981.

Phillips N, Ryan M, Bond B, McDowell N, Hinckley T, Čermák J. 2003. Reliance on stored water increases with tree size in three species in the Pacific Northwest. *Tree Physiology* **23**, 237–245.

Phillips NG, Oren R, Licata J, Linder S. 2004. Time series diagnosis of tree hydraulic characteristics. *Tree Physiology* **24**, 879–890.

Prieto I, Armas C, Pugnaire F. 2012. Water release through plant roots: new insights into its consequences at the plant and ecosystem level. *New Phytologist* **193**, 830–841.

Prieto I, Kikvidze Z, Pugnaire F. 2010. Hydraulic lift: soil processes and transpiration in the Mediterranean leguminous shrub *Retama sphaerocarpa* (L.) Boiss. *Plant and Soil* **329**, 447–456.

Scholz FG, Bucci SJ, Goldstein G, Moreira MZ, Meinzer FC, Domec J-C, Villalobos-Vega R, Franco AC, Miralles-Wilhelm F. 2008. Biophysical and life-history determinants of hydraulic lift in Neotropical savanna trees. *Functional Ecology* **22**, 773–786.

Schulze ED, Čermák J, Matyssek R, Penka M, Zimmermann R, Vasícek F, Gries W, Kučera J. 1985. Canopy transpiration and water fluxes in the xylem of the trunk of *Larix* and *Picea* trees a comparison of xylem flow, porometer and cuvette measurements. *Oecologia* **66**, 475–483.

Schymanski S, Sivapalan M, Roderick M, Beringer J, Hutley L. 2008. An optimality-based model of the coupled soil moisture and root dynamics. *Hydrology and Earth System Sciences Discussions* **12**, 913–932.

Siqueira M, Katul G, Porporato A. 2008. Onset of water stress, hysteresis in plant conductance, and hydraulic lift: scaling soil water dynamics from millimeters to meters. *Water Resources Research* **44**, W01432.

Sparks J, Black R. 1999. Regulation of water loss in populations of *Populus trichocarpa*: the role of stomatal control in preventing xylem cavitation. *Tree Physiology* **19**, 453–459.

Sperry JS, Love DC. 2015. What plant hydraulics can tell us about responses to climate-change droughts. *New Phytologist* **207**, 14–27.

Sperry JS, Tyree MT. 1990. Water-stress-induced xylem embolism in three species of conifers. *Plant, Cell & Environment* **13**, 427–436.

Stratton L, Goldstein G, Meinzer FC. 2000. Stem water storage capacity and efficiency of water transport: their functional significance in a Hawaiian dry forest. *Plant, Cell & Environment* **23**, 99–106.

Taneda H, Tateno M. 2011. Leaf-lamina conductance contributes to an equal distribution of water delivery in current-year shoots of kudzu-vine shoot, pueraria lobata. *Tree Physiology* **31**, 782–794.

Tuzet A, Perrier A, Leuning R. 2003. A coupled model of stomatal conductance, photosynthesis and transpiration. *Plant, Cell & Environment* **26**, 1097–1116.

Tyree MT. 1988. A dynamic model for water flow in a single tree: evidence that models must account for hydraulic architecture. *Tree Physiology* **4**, 195–217.

Tyree MT, Ewers FW. 1991. The hydraulic architecture of trees and other woody plants. *New Phytologist* **119**, 345–360.

Tyree MT, Sperry J. 1989. Vulnerability of xylem to cavitation and embolism. *Annual Review of Plant Biology* **40**, 19–36.

Tyree MT, Yang S. 1990. Water-storage capacity of *Thuja*, *Tsuga* and *Acer* stems measured by dehydration isotherms. *Planta* **182**, 420–426.

Tyree MT, Zimmermann MH. 2002. *Xylem structure and the ascent of sap*. Berlin, Germany: Springer.

Tyree MT, Davis S, Cochard H. 1994. Biophysical perspectives of xylem evolution: is there a tradeoff of hydraulic efficiency for vulnerability to dysfunction? *IAWA Journal* **15,** 335–360.

Vogel T, Dohnal M, Dusek J, Votrubova J, Tesar M. 2013. Macroscopic modeling of plant water uptake in a forest stand involving root-mediated soil water redistribution. *Vadose Zone Journal* **12**. doi: 10.2136/vzj2012.0154.

Volpe V, Marani M, Albertson JD, Katul GG. 2013. Root controls on water redistribution and carbon uptake in the soil–plant system under current and future climate. *Advances in Water Resources* **60**, 110–120.

Wang X, Tang C, Guppy C, Sale PWG. 2009. The role of hydraulic lift and subsoil P placement in P uptake of cotton (*Gossypium hirsutum*L.). *Plant and Soil* **325**, 263–275.

Waring R, Running S. 1978. Sapwood water storage: its contribution to transpiration and effect upon water conductance through the stems of old-growth Douglas-fir. *Plant, Cell & Environment* **1**, 131–140.

Waring R, Whitehead D, Jarvis P. 1979. The contribution of stored water to transpiration in Scots pine. *Plant, Cell & Environment* **2**, 309–317.

Warren JM, Meinzer FC, Brooks JR, Domec JC. 2005. Vertical stratification of soil water storage and release dynamics in Pacific Northwest coniferous forests. *Agricultural and Forest Meteorology***130**, 39–58.

Yoder CK, Nowak RS. 1999. Hydraulic lift among native plant species in the Mojave Desert. *Plant and Soil* **215**, 93–102.

Zang D, Beadle C, White D. 1996. Variation of sapflow velocity in *Eucalyptus globulus* with position in sapwood and use of a correction coefficient. *Tree Physiology* **16**, 697–703.
Zimmermann MH. 1983. *Xylem structure and the ascent of sap*. Berlin, Germany: Springer.

Supporting Information

Please note: Wiley Blackwell are not responsible for the content or functionality of any Supporting Information supplied by the authors. Any queries (other than missing material) should be directed to the *New Phytologist* Central Office.

Filename	Description
nph14273-sup-0001-MethodsS1-S3.pdfPDF document, 595.1 KB	**Methods S1** Model parameterization for the eight scenarios. **Methods S2** Comparisons between model calculations and measured sap flux of a loblolly pine tree (*Pinus taeda*). **Methods S3** Summary of modeled results.

Please note: The publisher is not responsible for the content or functionality of any supporting information supplied by the authors. Any queries (other than missing content) should be directed to the corresponding author for the article.